Aalto University

OPEN ACCESS

This is an electronic reprint of the original article.
This reprint may differ from the original in pagination and typographic detail.

Marín-Suárez, Marco; Peltonen, Joonas T.; Golubev, Dmitry S.; Pekola, Jukka P.

An electron turnstile for frequency-to-power conversion

Published in:
Nature Nanotechnology

DOI:
10.1038/s41565-021-01053-5

Published: 01/03/2022

Document Version
Peer-reviewed accepted author manuscript, also known as Final accepted manuscript or Post-print

Please cite the original version:
Marín-Suárez, M., Peltonen, J. T., Golubev, D. S., & Pekola, J. P. (2022). An electron turnstile for frequency-to-power conversion. *Nature Nanotechnology*, *17*(3), 239-243. https://doi.org/10.1038/s41565-021-01053-5

This material is protected by copyright and other intellectual property rights, and duplication or sale of all or part of any of the repository collections is not permitted, except that material may be duplicated by you for your research use or educational purposes in electronic or print form. You must obtain permission for any other use. Electronic or print copies may not be offered, whether for sale or otherwise to anyone who is not an authorised user.

Supporting Information
An electron turnstile for frequency to power conversion

Marco Marín-Suárez,[1,*] Joonas T. Peltonen,[1] Dmitry S. Golubev,[1] and Jukka P. Pekola[1,2]

[1] *Pico group, QTF Centre of Excellence, Department of Applied Physics, Aalto University, FI-000 76 Aalto, Finland*
[2] *Moscow Institute of Physics and Technology, 141700 Dolgoprudny, Russia*

S1. DEVICE CHARACTERIZATION AND TURNSTILE DEMONSTRATION

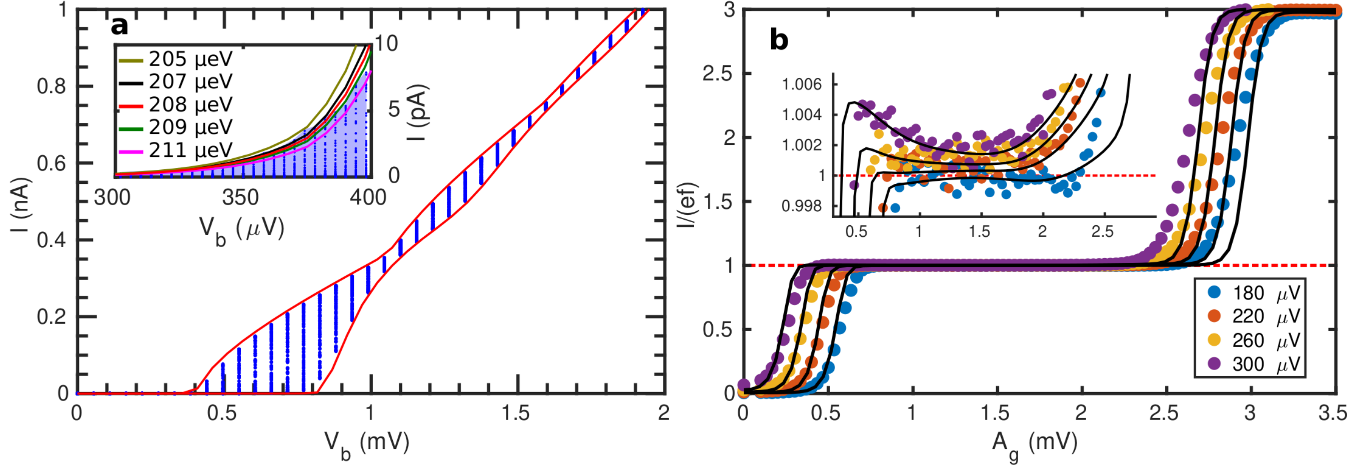

FIG. S1. **Device characterization and turnstile behaviour.** (a) DC IV curves for the measured sample. Red lines are simulations for the envelope bracketing experimental current at all the gate voltage values shown by the blue dots. (b) Typical turnstile measurements (dots) for the tested sample at $f = 20\,\mathrm{MHz}$; black lines are simulations. Here the current is measured against the gate driving amplitude A_{g}, the dashed red line illustrates the ideal value of current $I = ef$. Inset: close-up of the plateaus around $I = ef$.

The device parameters of the SET used for FPC were estimated from a DC measurement in which the bias voltage V_{b} is swept at the same time as a DC gate voltage. These measurements are shown in Fig. S1a as blue dots, red lines are the maximum and minimum transistor currents with respect to gate voltage calculated from a simple Markovian master equation on the discrete island charging events (described in Section S4) using $\Delta = 208\,\mu\mathrm{eV}$, charging energy $E_{\mathrm{c}} = 1.2\Delta$, total normal-state tunnel resistance $R_{\mathrm{T}} = 1.36\,\mathrm{M}\Omega$, ratio between resistances $R_{\mathrm{L}}/R_{\mathrm{R}} = 0.65$ and Dynes parameter [1] $\eta = 2.75 \times 10^{-4}$ as SET parameters, also a gate capacitance of $C_{\mathrm{g}} = 0.12\,\mathrm{fF}$ was measured. Because of the importance of knowing Δ precisely in frequency to power conversion, we inspect how the tunnelling current near the threshold voltage changes with it in order to estimate an uncertainty. This comparison is shown in the inset, whose gate modulation range is highlighted by a blue shade for clarity. From this, we conclude that, in our case, the superconducting gap measurement has an uncertainty of $< 1\%$ in the current realization.

In Figure S1b we demonstrate that this SET emits single-electron currents when voltage-biased and the gate is periodically driven. Here, a typical measurement is shown: the gate voltage is of the form $V_{\mathrm{g}} = V_{0\mathrm{g}} + A_{\mathrm{g}} \sin(2\pi f t)$, $V_{0\mathrm{g}}$ tuned at gate open position. One sees that the average measured current is around $I = ef$ for several gate amplitudes and V_{b} values when $V_{\mathrm{b}} \neq 0$. Solid black lines show results of simulations of the Markovian equation with the previously determined SET parameters. The inset shows that our calculations follow closely the measured current.

* marco.marinsuarez@aalto.fi

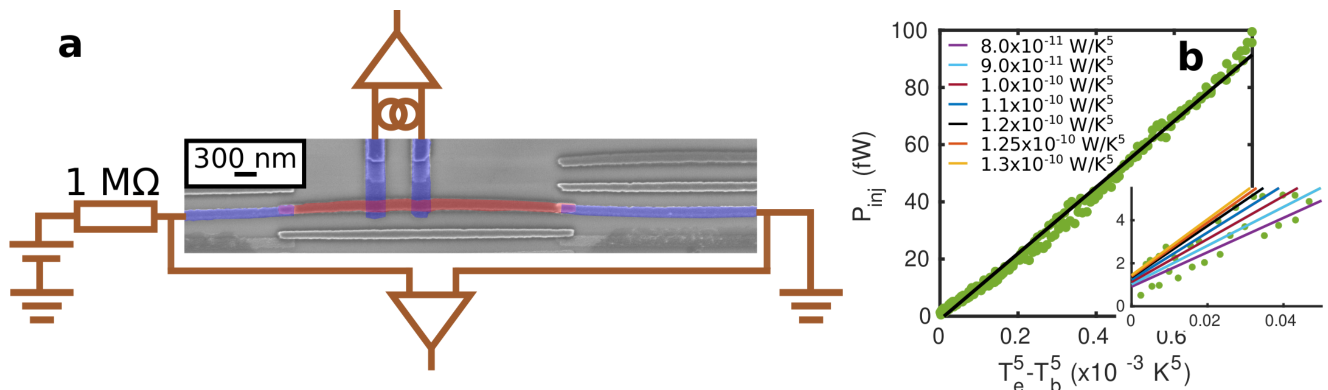

FIG. S2. **Bolometer characterization.** (a) Colored scanning electron micrograph of the device for measuring the electron-phonon coupling constant of the Cu strip (light red) along with the respective experimental setup. Light blue depicts superconducting Al. Dimensions of the normal-metal are nominally the same as in the measured device, which was evaporated during the same deposition on a different chip. (b) Measured injected power (green dots) against the difference of the 5th powers of the electron and bath temperatures. Black line is a linear fit to the data. The inset shows different linear fits with different values of $\Sigma\mathcal{V}$ in the power range of interest for our applications.

S2. BOLOMETER CHARACTERIZATION

In order to convert the measured temperature into the dissipated power P through the conventional normal-metal electron-phonon interaction model, e.g., $P = \Sigma\mathcal{V}\left(T_\mathrm{e}^5 - T_\mathrm{b}^5\right)$, it is necessary to determine the quantity $\Sigma\mathcal{V}$. Since $\mathcal{V}$ is the volume of the normal-metal, it is reasonable to use the nominal values. However, since we have an overlap between the normal-metal and the superconductor in the clean SN contact of about $195\,\mathrm{nm} \times 112\,\mathrm{nm}$ we measure the value $\Sigma\mathcal{V}$ to avoid uncertainties due to the qp relaxation in this region. This *in-situ* calibration is important because we need a quantitative calibration for the actual device in the experiment. To achieve this, a Cu strip of nominally equal volume (see Fig. S2a) was deposited on the same chip as the main samples over the same ground planes. Although the calibration of the bolometer was done on a different chip, its metal deposition was done at the same time as the measured sample to guarantee an identical behaviour of the Cu heat dissipation. Aluminium was evaporated to form SN contacts and NIS probes. The latter allow measuring the copper electronic temperature T_e as in the main sample, while the former allow the injection of a known current and measuring accurately the voltage drop in the normal-metal due to this current.

In Fig. S2a a known current I is generated by applying a voltage to a $1\,\mathrm{M}\Omega$ resistor, simultaneously the voltage drop V in the normal metal is measured in a four-probe geometry. With this setup, the dissipated power is easily determined as Joule heating $P = IV$ which by continuity is also given by $P = \Sigma\mathcal{V}\left(T_\mathrm{e}^5 - T_\mathrm{b}^5\right)$. Since we also have experimental access to T_e and bath temperature T_b it is possible to plot the power against $T_\mathrm{e}^5 - T_\mathrm{b}^5$ as the green dots of Fig. S2b, notice that the dependence is approximately linear confirming the exponent. The plotted data are well caught by a linear fitting (black line in Fig. S2b) with a slope $\Sigma\mathcal{V} = 1.2 \times 10^{-10}\,\mathrm{WK}^{-5}$. By comparing the data with different slopes, an uncertainty interval for $\Sigma\mathcal{V}$ can be found. We conclude that $\Sigma\mathcal{V} = 113 \pm 13\,\mathrm{pWK}^{-5}$. We have decided to use the slope of the black line for plotting data merely for presentation purposes, since it is within the estimated uncertainty. Data converted to power match the Markovian model within the error interval. The present calibration shows that the slope for low powers is slightly smaller than for larger ones. In future experiments this needs to be studied further. The actual FPC measurements are performed in the power range $\lesssim 5\,\mathrm{fW}$.

S3. BOLOMETER RESPONSE CALIBRATION

The thermometer responses were calibrated by comparing the measured voltage drop through the probe SINIS junctions V_SINIS with the bath temperature T_b measured by a ruthenium oxide resistor (Scientific Instruments, Inc., model RO-600) previously calibrated against a Coulomb blockade thermometer. This procedure was done by carefully controlling that no external heat sources (other than the environment) heated the bolometers. Therefore, a turnstile gate amplitude $A_\mathrm{g} = 0$ was applied throughout the whole calibration procedure. The results of these measurements are shown in Figs. S3a and S3b for the bolometer in contact with the left and right leads, respectively, as blue dots. There is a clear linear region whose slope is given by the red lines. We carefully keep the bath temperature and the

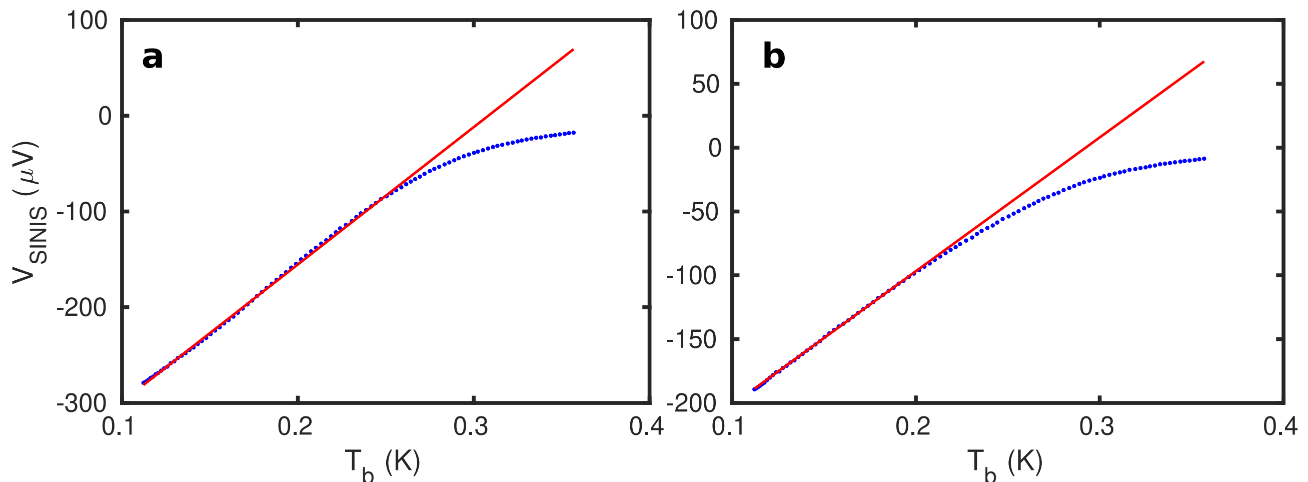

FIG. S3. **Bolometer response calibration.** (a) Response of the left lead bolometer (blue dots) to a bath temperature $T_{\rm b}$ and a fit to the linear region of the thermometer (red line). (b) As in (a) for the right lead.

response temperature due to turnstile power injection within the linear region during the main measurements.

S4. NUMERICAL CALCULATIONS

In steady state (for DC calculations) and since the charging events n are discrete one can express Eq. (3) as the matrix equation [2]

$$A\mathbf{p} = \mathbf{0}, \tag{S1}$$

where $p_i = p(n_i)$, $A_{ii} = -\sum_{j\neq i}\gamma_{ij}$ and $A_{ij} = \gamma_{ij}$ for $i \neq j$. Extending to two leads, as for an SET, the total transition rates are given by $\gamma_{nn'} = \Gamma^{\rm L}_{n\to n'}(\varepsilon) + \Gamma^{\rm R}_{n\to n'}(\varepsilon)$. Here, Γ is the transition rate between individual charging states n and n', L denotes events through the left junction and R similarly stands for the right one. Finally, ε is the energy change of the process given by

$$\varepsilon^{\pm,{\rm L/R}}_{1e}(n,V) = \mp 2E_{\rm c}(n - n_{\rm g} \pm 0.5) \pm eV_{\rm L/R} \tag{S2}$$

$$\varepsilon^{\pm,{\rm L/R}}_{2e}(n,V) = \mp 4E_{\rm c}(n - n_{\rm g} \pm 1) \pm 2eV_{\rm L/R}, \tag{S3}$$

for single-electron ($1e$) and two-electron ($2e$) tunnelling, respectively. Here $V_{\rm L} = \kappa_{\rm L}V_{\rm b}$ and $V_{\rm R} = -\kappa_{\rm R}V_{\rm b}$, $\kappa_{\rm L/R}$ is the ratio between the junction capacitance and the total capacitance, $V_{\rm b}$ is the bias voltage applied between the leads of the transistor. In Eqs. (S2) and (S3) n is the initial island excess charge, $n_{\rm g}$ is the charge number induced by the gate voltage, $E_{\rm c}$ is the charging energy and $+\,(-)$ designates tunnelling to (from) the island.

The explicit expression for the rates depends on the specific system and on the transition processes taken into account. Considering transitions in NIS junctions and only single-electron and two-electron Andreev processes, we have

$$\Gamma^{\rm L/R}_{n\to n\pm 1}(\varepsilon) = \frac{1}{e^2 R_{\rm L/R}} \int dE\, n_{\rm s}(E)\left(1 - f_{\rm N}(E+\varepsilon)\right) f_{\rm S}(E) \tag{S4}$$

for single-electron tunnelling, and

$$\begin{aligned}\Gamma^{\rm L/R}_{n\to n\pm 2}(\varepsilon) = \frac{\hbar\Delta^2}{16\pi e^4 R^2_{\rm L/R}\mathcal{N}} &\int dE\, f_{\rm N}(E - \varepsilon/2)\, f_{\rm N}(-E - \varepsilon/2)\,\times \\ &\left|a(E + E_{\rm c} - i\delta/2) + a(-E + E_{\rm c} - i\delta/2)\right|^2\end{aligned} \tag{S5}$$

for Andreev tunnelling. Here, ε is the corresponding energy change from Eqs. (S2) or (S3), respectively.

In Eqs. (S4) and (S5), Δ is the superconducting gap of the leads, $R_{\rm L/R}$ is the junction normal-state tunnel resistance and $\mathcal{N}$ is the number of conduction channels which can be written as $A/A_{\rm ch}$ with A being the junction area ($\approx$

49 nm × 63 nm for the measured device) and A_{ch} is the area of an individual channel (typically 30 nm^2). The term δ takes into account the energy of the intermediate (single-electron tunnelling) state which has a finite lifetime [3] and therefore can be estimated as $\hbar\sum_{\pm}\Gamma_{n\to n\pm1}$. However, in our simulations and in the regime of interest the precise value does not have an impact on the calculated Andreev tunnelling rates [4]. We set a reasonable value of $\delta/\Delta = 10^{-5}$. Additionally, f_{N} is the Fermi-Dirac distribution of the normal-metal island, f_{S} is that for the superconducting lead involved in the tunnelling event and n_s is the superconducting quasiparticle density of states given by

$$n_{\mathrm{s}}(E) = \left|\mathfrak{Re}\left(\frac{E/\Delta + i\eta}{\sqrt{(E/\Delta + i\eta)^2 - 1}}\right)\right|, \tag{S6}$$

here, η is the Dynes parameter which models subgap leaks [1, 5]. Furthermore,

$$a(x) = \frac{1}{\sqrt{x^2-\Delta^2}}\ln\left(\frac{\Delta - x + \sqrt{x^2-\Delta^2}}{\Delta - x - \sqrt{x^2-\Delta^2}}\right). \tag{S7}$$

Once the probability vector $\mathbf{p}$ is obtained by solving Eq. (S1), the current through the SET can be calculated as $I = \mathbf{b}\cdot\mathbf{p}$ with $b_i = e\left(\Gamma^{\mathrm{L}}_{i\to i+1} - \Gamma^{\mathrm{L}}_{i\to i-1}\right) + 2e\left(\Gamma^{\mathrm{L}}_{i\to i+2} - \Gamma^{\mathrm{L}}_{i\to i-2}\right)$. In order to get realistic results the temperature change of the island has to be taken into account. To do this, one calculates the power transferred in single-electron events to the normal island provided ε is constant

$$\dot{Q}^{\mathrm{N,L/R}}_{n\to n\pm1}(\varepsilon) = \frac{1}{e^2 R_{\mathrm{L/R}}}\int dE E n_{\mathrm{s}}(E-\varepsilon) f_{\mathrm{N}}(E)(1 - f_{\mathrm{S}}(E-\varepsilon)), \tag{S8}$$

where N refers to normal metal and ε is again the related energy change cost from Eq. (S2). The total power transferred to the island is calculated as $\dot{Q} = \mathbf{q}\cdot\mathbf{p}$ with $q_i = \dot{Q}^{\mathrm{N}}_{i\to i+1} + \dot{Q}^{\mathrm{N}}_{i\to i-1}$, where $\dot{Q}^{\mathrm{N}}_{i\to i\pm1} = \dot{Q}^{\mathrm{N,R}}_{i\to i\pm1} + \dot{Q}^{\mathrm{N,L}}_{i\to i\pm1}$. The heat flow to the phonons in the N island is governed by $\dot{Q}_{\mathrm{e-ph}} = \mathcal{V}\Sigma\left(T_{\mathrm{N}}^5 - T_{\mathrm{b}}^5\right)$ where $\mathcal{V}$ is the volume of the island ($\approx$ 930 nm × 105 nm × 40 nm for the measured device), Σ is the electron-phonon coupling constant ($\approx 8.4\times10^{9}\,\mathrm{WK^{-5}m^{-3}}$), T_{N} is the electron temperature of the island and T_{b} is the temperature of the phonon bath which is considered to be the same as the base temperature. Finally, the heat balance is $\dot{Q}_{\mathrm{e-ph}} = \dot{Q}$. This condition is used to solve for T_{N}.

A similar method can be applied during the turnstile operation [2]. If the period of the driving is τ then it is valid to assume that the steady state probability satisfies $p(t) = p(t+\tau)$. In order to solve for the probability the cycle is discretized in m intervals of length $\Delta t = \tau/m$, next the matrix $A(k\Delta t) = A_k$ is calculated for each interval as well as the $\mathbf{b}_k$ vector. If we now build the propagator

$$U(\tau) = \prod_{k=1}^{m}\exp(\Delta t A_k), \tag{S9}$$

then the initial probability is given by

$$U(\tau)\,\mathbf{p}(0) = \mathbf{p}(0), \tag{S10}$$

since for a periodic driving $\mathbf{p}(0) = \mathbf{p}(\tau)$.

A more useful form of the propagator is given by

$$\tilde{U}(\tau) = \prod_{k=1}^{m}\exp\left(\Delta t\tilde{A}_k\right), \tag{S11}$$

where

$$\tilde{A}_k = \begin{bmatrix} A_k & \mathbf{0} \\ \mathbf{b}_k^{\mathrm{T}} & 0 \end{bmatrix}. \tag{S12}$$

In Eq. (S12) $\mathbf{0}$ is a vector of zeros with the appropriate dimensions. This way Eq. (4) can be reformulated in terms of the augmented rate matrix $\left(\tilde{A}_k\right)$ and a new probability vector $\tilde{\mathbf{p}}(t) = [\mathbf{p}(t) \quad \langle q\rangle]^{\mathrm{T}}$, where $\langle q\rangle$ is the average charge transferred during one cycle. The final propagator can be decomposed as

$$\tilde{U}(\tau) = \begin{bmatrix} U & \mathbf{0} \\ \mathbf{U}_{\mathrm{b}} & 0 \end{bmatrix}. \tag{S13}$$

Then, Eq. (S10) is reformulated in terms of this new propagator and the average charge is obtained as $\langle q\rangle = \mathbf{U}_\mathrm{b}\cdot\mathbf{p}(0)$. The average current pumped is $I=\langle q\rangle/\tau$. The energy injected to the left/right superconducting leads is calculated by replacing $\mathbf{b}$ by $\mathbf{q}^{\mathrm{L/R}}$ in Eq. (S12) with $q_i^{\mathrm{L/R}} = \dot{Q}^{\mathrm{S,L/R}}_{i\to i+1} + \dot{Q}^{\mathrm{S,L/R}}_{i\to i-1}$, where in turn $\dot{Q}^{\mathrm{S,L/R}}_{i\to i\pm1} = \dot{Q}^{\mathrm{N,L/R}}_{i\to i\pm1} - \varepsilon^{\pm,\mathrm{L/R}}_{1e}\Gamma^{\mathrm{L/R}}_{i\to i\pm1}$. Furthermore, the probability vector is redefined as $\tilde{\mathbf{p}}(t) = \begin{bmatrix}\mathbf{p}(t) & \langle E_{\mathrm{L/R}}\rangle\end{bmatrix}^\mathrm{T}$, where $\langle E_{\mathrm{L/R}}\rangle$ is the average injected energy to the left/right lead and is obtained as $\langle E_{\mathrm{L/R}}\rangle = \mathbf{U}^{\mathrm{L/R}}_\mathrm{q}\cdot\mathbf{p}(0)$, where $\mathbf{U}^{\mathrm{L/R}}_\mathrm{q}$ is retrieved from a decomposition similar to Eq. (S13). Finally, the average injected power to the left/right lead is given by $P_{\mathrm{L/R}} = \langle E_{\mathrm{L/R}}\rangle/\tau$.

S5. FPC AND BOLOMETER NOISE COMPARISON

From analogy to the current shot noise in single-electron pumps [6] and assuming that it is much more probable to have extra tunnellings than missed tunnellings; we estimate that the signal-to-noise ratio in FPC follows

$$\mathrm{SNR}_\mathrm{FPC} \propto \sqrt{\frac{P_\mathrm{ideal} f\tau}{P-P_\mathrm{ideal}}}. \tag{S14}$$

Where P_ideal is the power produced with no extra/missed tunnelling events, f the operation frequency, τ the averaging time and P the real (with tunnelling errors) produced power.

On the other hand, there is noise in the power detection by the bolometer. The noise power associated with the power dissipation is given by

$$S_P = 2k_\mathrm{B}T^2G_\mathrm{th}. \tag{S15}$$

Here k_B is the Boltzmann constant, T the bolometer temperature and G_th the linear response thermal conductance of the bolometer taken as $G_\mathrm{th} = 5\Sigma\mathcal{V}T^4$. The bolometer power dissipation signal-to-noise ratio is the given by

$$\mathrm{SNR}_\mathrm{bolo} = \frac{P}{\sqrt{S_P/\tau}} = \frac{P}{T}\sqrt{\frac{\tau}{2k_\mathrm{B}G_\mathrm{th}}}. \tag{S16}$$

P is also the power produced by FPC. At low frequencies ($f \ll G_\mathrm{th}T/(10\Delta)$) we can assume that $T\approx T_\mathrm{b}$.

In Fig. S4 Eqs. (S14) and (S16) are depicted as function of the driving frequency for a device with the same parameters to the one simulated in Fig. 3f, but with $T_\mathrm{N} = 100\,\mathrm{mK}$. This higher island temperature makes $P/(2\Delta f) > 1$ and higher as shown in Fig. S4c. It is also evident that $\mathrm{SNR}_\mathrm{bolo} \ll \mathrm{SNR}_\mathrm{FPC}$, hence the bolometer detection noise is dominant over the FPC one at low frequencies (in fact, even when f is large and $T\approx T_\mathrm{b}$ is not valid). While this holds independent of the Dynes parameter η value (see Fig. S4), at low frequencies FPC P is below Eq. (1) for devices with high η. For these structures the probability of an electron leaking into subgap states $\varepsilon < \Delta$ increases with decreasing driving frequency. Therefore, at low frequencies, when $\mathrm{SNR}_\mathrm{bolo}$ decreases, the main impediment for accurate FPC is having non-vanishing η.

S6. CALCULATION OF $P_\mathrm{R}/P_\mathrm{L}$ AT $V_\mathrm{b} = 0\,\mathrm{V}$

In general, Eqs. (S4) and (S8) can be expressed as

$$\Gamma^{\mathrm{L/R}}_{n\to n\pm1} = \frac{1}{R_{\mathrm{L/R}}}\xi^{\mathrm{L/R}}_{n\to n\pm1}\left(\varepsilon^{\pm,\mathrm{L/R}}_{1e}(n,V_\mathrm{b}), T_\mathrm{N}, T_\mathrm{S}^{\mathrm{L/R}}\right) \tag{S17}$$

$$\dot{Q}^{\mathrm{N,L/R}}_{n\to n\pm1} = \frac{1}{R_{\mathrm{L/R}}}\dot{q}^{\mathrm{N,L/R}}_{n\to n\pm1}\left(\varepsilon^{\pm,\mathrm{L/R}}_{1e}(n,V_\mathrm{b}), T_\mathrm{N}, T_\mathrm{S}^{\mathrm{L/R}}\right). \tag{S18}$$

Where, T_N is the temperature of the normal-metal island and $T_\mathrm{S}^{\mathrm{L/R}}$ the quasiparticle temperature of the left/right lead. The quantities ξ and $\dot{q}$ are functions of the island charge state and temperatures as well as bias voltage. When $V_\mathrm{b} = 0$ the energy change of the process becomes

$$\varepsilon^{\pm,\mathrm{L}}_{1e}(n) = \varepsilon^{\pm,\mathrm{R}}_{1e}(n) = \varepsilon = \pm 2E_\mathrm{c}(n - n_\mathrm{g} \pm 0.5). \tag{S19}$$

Therefore, and making the important but reasonable assumption that $T_\mathrm{S}^\mathrm{L} = T_\mathrm{S}^\mathrm{R}$, we have that $\xi^\mathrm{L}_{n\to n\pm1} = \xi^\mathrm{R}_{n\to n\pm1} = \xi_{n\to n\pm1}$ and $\dot{q}^{\mathrm{N,L}}_{n\to n\pm1} = \dot{q}^{\mathrm{N,R}}_{n\to n\pm1} = \dot{q}^{\mathrm{N}}_{n\to n\pm1}$. As a consequence, the same reasoning can be done to $\dot{Q}^{\mathrm{S,L/R}}_{n\to n\pm1}$, therefore

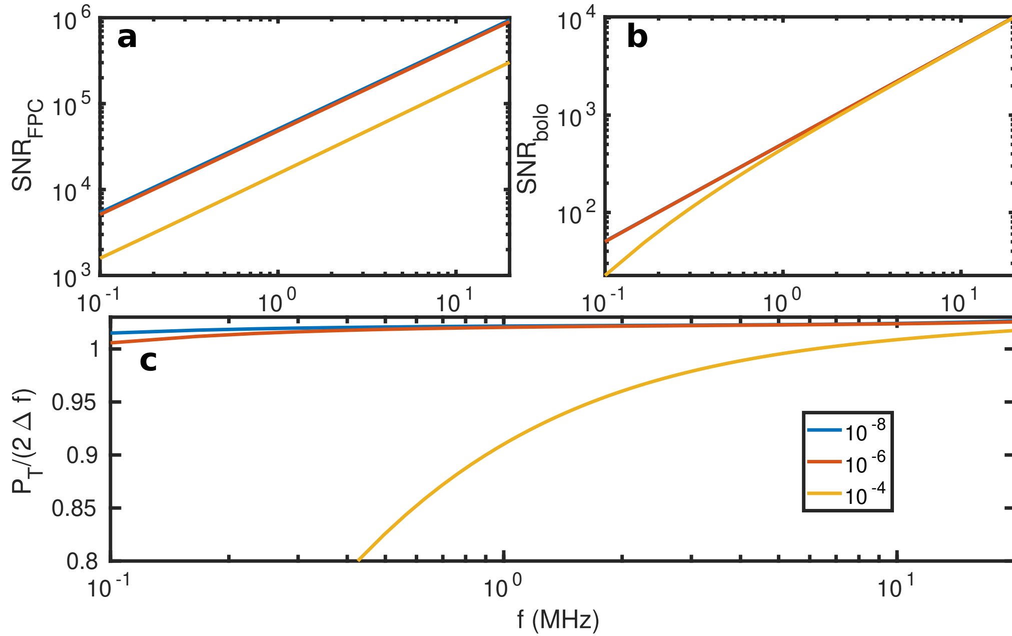

FIG. S4. **FPC and bolometer noise.** (a) FPC signal-to-noise ratio, the colors correspond to the legend in panel (c) and show the Dynes parameter. (b) Bolometer power detection signal-to-noise ratio, the blue curve is hidden behind the red one. (c) Total power produced by FPC.

the total power injected to the left/right superconductor is given by

$$P_{\mathrm{L/R}} = \frac{1}{R_{\mathrm{L/R}}} \sum_n p_n \left(\dot{q}^{\mathrm{S}}_{n\to n+1} + \dot{q}^{\mathrm{S}}_{n\to n-1} \right). \tag{S20}$$

Where $\dot{q}^{\mathrm{S}} = \dot{q}^{\mathrm{N}} - \varepsilon\xi$. The ratio is then given by

$$\frac{P_{\mathrm{R}}}{P_{\mathrm{L}}} = \frac{1/R_{\mathrm{R}} \sum_n p_n \left(\dot{q}^{\mathrm{S}}_{n\to n+1} + \dot{q}^{\mathrm{S}}_{n\to n-1} \right)}{1/R_{\mathrm{L}} \sum_n p_n \left(\dot{q}^{\mathrm{S}}_{n\to n+1} + \dot{q}^{\mathrm{S}}_{n\to n-1} \right)} = \frac{R_{\mathrm{L}}}{R_{\mathrm{R}}}. \tag{S21}$$

This result is also true for the experiment on average as shown in Figs. 3g and 3h.

S7. LOSS OF ENERGY SELECTIVITY AT HIGHER FREQUENCIES

Recall from Section S4 and Eq. (5) that the instantaneous power can be calculated as

$$P_{\mathrm{R/L}} = \sum_n p\,(n) \left(\dot{Q}^{\mathrm{S,R/L}}_{n\to n+1} + \dot{Q}^{\mathrm{S,R/L}}_{n\to n-1} \right), \tag{S22}$$

and that the integrals $\dot{Q}^{\mathrm{S,R/L}}_{n\to n+1}$ depend on the energy change of the electron involved in the charging event, which in turn depends on time in the turnstile operation. As mentioned in the main manuscript for an electron tunnelling into the island, this energy is given explicitly by

$$\varepsilon = 2E_{\mathrm{c}}\,(0.5 - n_{\mathrm{g}})\,, \tag{S23}$$

when $V_{\mathrm{b}} = 0$. Under sinusoidal gate driving $n_{\mathrm{g}} = 0.5 + C_{\mathrm{g}}A_{\mathrm{g}}/e \sin(2\pi f t)$, and t is now a parameter for $P = P_{\mathrm{L}} + P_{\mathrm{R}}$ and ε.

Figure S5 shows a parametric curve of the total power P injected versus ε under the same conditions as the results of Fig. 3e. Here, as well, it is possible to see that only electrons within a narrow energy band around the gap tunnel (inject energy) when the driving frequency is low and sharp power peaks around $\varepsilon = \Delta$ appear. As the driving

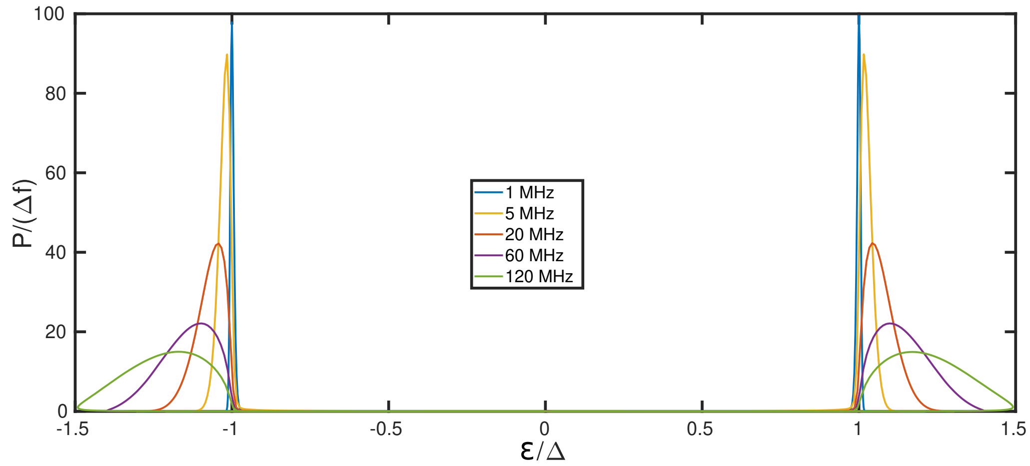

FIG. S5. **Change of the energy selectivity with driving frequency.** Instantaneous total injected power calculated under the same conditions as Fig. 3e but for different driving frequencies against the electron energy change when jumping into the island. Showing how electrons of higher energy can tunnel and selectivity is progressively lost the higher the driving rate.

frequency increases and the rate of change of ε becomes comparable to the tunnelling rates, these peaks spread more in ε, indicating that electrons with higher energies are tunnelling and therefore increasing the average injected power.

---

[1] Dynes, R. C., Narayanamurti, V. & Garno, J. P. Direct measurement of quasiparticle-lifetime broadening in a strong-coupled superconductor. *Phys. Rev. Lett.* **41**, 1509–1512 (1978).

[2] Saira, O.-P. *Electrostatic control of quasiparticle transport in superconducting hybrid nanostructures; Kvasipartikkelien kuljetuksen hallinta hilajännitteellä nanomittakaavan suprajohde-normaalimetalli-hybridirakenteissa*. Ph.D. thesis, Aalto University (2013). URL `http://urn.fi/URN:ISBN:978-952-60-5076-8`.

[3] Averin, D. V. & Pekola, J. P. Nonadiabatic charge pumping in a hybrid single-electron transistor. *Phys. Rev. Lett.* **101**, 066801 (2008).

[4] Maisi, V. F. *Andreev tunneling and quasiparticle excitations in mesoscopic normal metal - superconductor structures*. Doctoral thesis, Aalto University. School of Science (2014). URL `http://urn.fi/URN:ISBN:978-952-6682-11-2`.

[5] Pekola, J. P. *et al.* Environment-assisted tunneling as an origin of the Dynes density of states. *Phys. Rev. Lett.* **105**, 026803 (2010).

[6] Maire, N. *et al.* Noise measurement of a quantized charge pump. *Applied Physics Letters* **92**, 082112 (2008).